Investigation of longitudinal ^{31}P relaxation in metal selenophosphate compounds

Christian G. Canlas, Rajendra B. Muthukumaran, Mercouri G. Kanatzidis, and David P. Weliky[*]

Department of Chemistry, Michigan State University, East Lansing, MI 48824-1322, USA

Abstract

Molten salt syntheses yield a rich variety of metal selenophosphate compounds which have a wide range of ^{31}P T_1 longitudinal relaxation times (20–3000 s). There is a qualitative positive correlation between squared dipolar couplings and $1/T_1$, suggesting that these interactions contribute to relaxation. However, two of the compounds, $K_2CdP_2Se_6$ and $Rb_2CdP_2Se_6$, have T_1 which are significantly shorter than what is expected from dipolar couplings. The ESR spectra of these compounds show the presence of unpaired electrons which may accelerate the rate of ^{31}P relaxation. The importance of relaxation in application of ^{31}P NMR to these systems is demonstrated in analysis of the mixture of crystalline products formed in a $Ag_4P_2Se_6$ synthesis. At short relaxation delays, the NMR intensities are non-quantitative and overestimate the concentration of an Ag_7PSe_6 impurity.
© 2003 Elsevier Inc. All rights reserved.

Keywords: Selenophosphates; 31P; Longitudinal; Relaxation; T1; Dipolar; Couplings; Paramagnetic; ESR; NMR

1. Introduction

Chalcophosphates are compounds with oxidized phosphorus and at least one P–Q bond, where Q = S or Se. To date, no examples with Q = Te exist in the literature. These compounds exhibit an impressively rich structural diversity because of the large number of stable $[P_yQ_z]^{n-}$ building blocks that can be stabilized and the variety of binding modes in which they can engage [1]. Thio- and selenophosphates are still a

*Corresponding author. Tel.: 517-355-9715 x281; fax: 517-353-1793.
E-mail address: weliky@cem.msu.edu (D.P. Weliky).

relatively small group of compounds compared to the huge class of oxophosphates. The latter are important in the areas of catalysis, ceramics, glasses, and molecular sieves. Many thio- and seleno-phosphates however also exhibit promising and unique properties such as intercalation chemistry, ion-exchange, and magnetic and optical phenomena [2–5].

Among the first chalcophosphate compounds to be studied were the $M_2P_2Q_6$ class (M = divalent metal) which features the ethane-like $[P_2Q_6]^{4-}$ ligand [6] as well as M_3PQ_4, and MPQ_4 [7] with $[PQ_4]^{3-}$ ligands (M = monovalent or trivalent metal). Various other examples of $[P_yQ_z]^{n-}$ containing materials also exist [8–10]. Interesting properties and uses exhibited by some $[P_2Q_6]^{4-}$ containing compounds are: ferroelectricity for use in memory devices ($Sn_2P_2S_6$, $CuInP_2S_6$) [11, 12]; non-linear optical properties ($Mn_2P_2S_6$) [5]; and photoconductivity ($In_{1.33}P_2Se_6$) [13, 14].

Given the plethora of new chalcophosphate phases discovered in the last decade, and the variety of novel structural types, bonding modes, and chalcophosphate anions, it would be particularly desirable to study the NMR properties of these phases. Studies of this type are relatively rare [12, 15–18] and a wide compilation of NMR data on $[P_xQ_y]^{n-}$ anions should yield new insights into chalcophosphate compounds. In a previous NMR study, we focused on correlations between ^{31}P chemical shifts (CSs) or chemical shift anisotropies (CSAs) and local structure and bonding in metal selenophosphates [19]. We observed an important correlation between the ^{31}P CS and the presence or absence of a P–P bond in the selenophosphate anion. In the present paper, we investigate longitudinal ^{31}P relaxation in metal selenophosphate compounds and observe relaxation rates which range over two orders of magnitude. Unlike the CS and CSA, there does not appear to be a correlation between local anionic structure and relaxation rates. A combination of theoretical and experimental approaches suggests that much of the variation in relaxation rates can be correlated with: (1) dipolar couplings to surrounding nuclei; and (2) dipolar couplings to unpaired electrons associated with as-yet chemically unidentified paramagnetic impurities.

2. Materials and methods

2.1. Synthesis

P_2Se_5 was prepared by reacting stoichiometric amounts of the elements in an evacuated Pyrex tube at 300°C for 1 day, followed by a cool-down to 50°C over 2 h. Purity was assessed by X-ray powder diffraction analysis.

$Ag_4P_2Se_6$ [20], $Pb_2P_2Se_6$ [21], and Cu_3PSe_4 [22] were prepared by reacting stoichiometric amounts of the metal (Ag, Pb, Cu) with P_2Se_5 and elemental Se. The reaction took place in an evacuated quartz tube at 600°C for 1 day followed by a cool-down to 50°C over 12 h.

$KPbPSe_4$ and $RbPbPSe_4$ [23] were prepared from stoichiometric amounts of the alkali selenide (K_2Se or Rb_2Se), Pb metal, P_2Se_5, and elemental Se. The reactants

were heated in an evacuted quartz tube at $600\,°C$ for 1 day and cooled down to $50\,°C$ over 12 h.

$K_2Cu_2P_4Se_{10}$ [24] was prepared from 0.3 mmol Cu, 0.9 mmol P, 0.3 mmol K_2Se, and 2.4 mmol Se. The reactants were heated at $570\,°C$ for 2 days followed by cooling at $21\,°C/h$. The residual flux was removed with *N,N*-dimethylformamide. After washing the remaining solid with diethyl ether, red-irregularly shaped crystals were obtained which were stable in air and water.

$K_4Pb(PSe_4)_2$ [23] was prepared as orange crystals from 0.15 mmol Pb, 0.225 mmol P_2Se_5, 0.6 mmol K_2Se, and 1.5 mmol Se. The reactants were heated at $500\,°C$ for 3 days followed by cooling at $10\,°C/h$.

$Rb_2CdP_2Se_6$ and $K_2CdP_2Se_6$ [25] were prepared from 0.25 mmol Cd, 0.75 mmol P_2Se_5, 1.0 mmol Rb_2Se or K_2Se, and 2.5 mmol Se with the same heating profile as was used for $K_4Pb(PSe_4)_2$. The residual flux was removed with *N,N*-dimethylformamide. After the remaining solid was washed with diethyl ether, dark yellow rod-like crystals were obtained, which were stable in air and water.

$Cs_4P_2Se_9$ [26] was synthesized from a mixture of 0.45 mmol P_2Se_5, 1.20 mmol Cs_2Se, and 3.0 mmol Se. The reactants were sealed under vacuum in a pyrex tube and heated to $490\,°C$ for four days followed by cooling to $150\,°C$ at $10\,°C/h$. The product crystals were red and were sensitive to air and water.

$Rb_4Ti_2P_6Se_{25}$ [26] was synthesized from a mixture of 0.2 mmol Ti, 0.4 mmol P_2Se_5, 0.4 mmol Rb_2Se, and 2 mmol Se. The reactants were sealed under vacuum in a pyrex tube and heated according to the same heating profile as $Cs_4P_2Se_9$. The residual flux was removed with *N,N*-dimethylformamide. After the remaining solid was washed with ether, black crystals were formed, which were stable in air and water. The original goal of this synthesis was to make $RbTiPSe_5$ but powder X-ray diffraction and elemental analysis on selected crystals showed that $Rb_4Ti_2P_6Se_{25}$ was the only crystalline product.

2.2. Physical measurements

Powder X-ray diffraction: Powder X-ray diffraction analyses were performed using an INEL CPS 120 powder diffractometer with graphite monochromatized Cu *K*α radiation. To assess sample purity, we visually compared the experimental powder diffraction pattern to a pattern calculated from a single-crystal structure. Visual inspection using a light microscope was also performed to assess the crystallinity of the sample.

NMR: The room temperature solid-state NMR measurements of these poly-crystalline compounds were taken on a 9.4 T NMR Spectrometer (Varian Infinity Plus) using a double-resonance magic angle spinning (MAS) probe. Samples were spun at 8–15 kHz using zirconia rotors of 4 mm outer diameter and 50 μl volume. Bloch decay spectra were taken with the excitation/detection channel tuned to ^{31}P at 161.39 MHz, a 4.5 μs 90° pulse (calibrated to ± 0.1 μs), and a relaxation delay which was varied over a range from 5 to 15,000 s. Each spectrum was processed with $\leqslant 100$ Hz line broadening and up to a tenth-order polynomial baseline correction. The spectra were referenced using 85% H_3PO_4 at 0 ppm.

Each compound ^{31}P longitudinal relaxation time (T_1) was determined from fits to the equation:

$$S(\tau) = S_o(1 - e^{-\tau/T_1}), \tag{1}$$

where τ is the relaxation delay time before pulsing, $S(\tau)$ is the integrated signal intensity (sum of isotropic peak and spinning sidebands), and S_o is a fitting parameter representing the signal intensity at infinite τ. Before each τ, the magnetization was nulled with a 90° pulse and subsequent rapid transverse dephasing. For each compound, there were typically at least two data sets and the experimental T_1 uncertainty was calculated from the variation in best-fit T_1 values among the different data sets. This variation was generally larger than the fitting uncertainty in the T_1 value of a single data set.

ESR: Spectra were obtained at X-band using a Bruker ER300E spectrometer equipped with a TE102 ESR cavity. An Oxford ESR-900 cryostat and ITC 502 temperature controller were used to maintain constant sample temperature. The external magnetic field strength was measured with a Bruker ER 035 M NMR Gaussmeter and the microwave frequency was determined with an EIP 25B frequency counter. The polycrystalline samples were contained in vacuum-sealed quartz tubes at 4.2 K.

3. Results and discussion

Fig. 1 summarizes the structural schemes for the different selenophosphate anions examined in this paper. ^{31}P solid-state NMR data are presented in Table 1, including the measured CS, CSA, and T_1 values. The CS and CSA measurements are described in a previous paper [19]. Briefly, Table 1 shows that the ^{31}P CS is correlated with the presence of P–P bonding in metal selenophosphate compounds. There are non-overlapping CS ranges of compounds with P–P bonds (20–100 ppm) and compounds without P–P bonds (−120 to −30 ppm). CSA measurements demonstrated that the CSAs of compounds containing $[PSe_4]^{3-}$ were significantly smaller than those of compounds containing any other ion. These CSA observations are most reasonably explained by the tetrahedral symmetry which is unique to $[PSe_4]^{3-}$.

3.1. Longitudinal relaxation rates

Fig. 2 displays experimental and best-fit buildup curves for (a) $Ag_4P_2Se_6$ and Ag_7PSe_6 and (b) $K_2CdP_2Se_6$. Fitting was done using Eq. (1) and yielded ^{31}P T_1 values of 3000, 1500, and 20 s, respectively. Among all of the compounds in the present study, $Ag_4P_2Se_6$ and $K_2CdP_2Se_6$ had the slowest and fastest relaxation rates, respectively. The T_1 values for compounds containing $[P_2Se_7]^{4-}$ and $[P_2Se_9]^{4-}$ were clustered between 600 and 800 s while those containing $[P_2Se_6]^{4-}$ ranged between 20 and 3000 s and those containing $[PSe_4]^{3-}$ ranged between 300 and 1500 s. Isostructural pairs such as $Rb_2CdP_2Se_6/K_2CdP_2Se_6$ and $RbPbPSe_4/KPbPSe_4$ exhibit

(a) $[P_2Se_6]^{4-}$

(b) $[PSe_4]^{3-}$

(c) $[P_4Se_{10}]^{4-}$

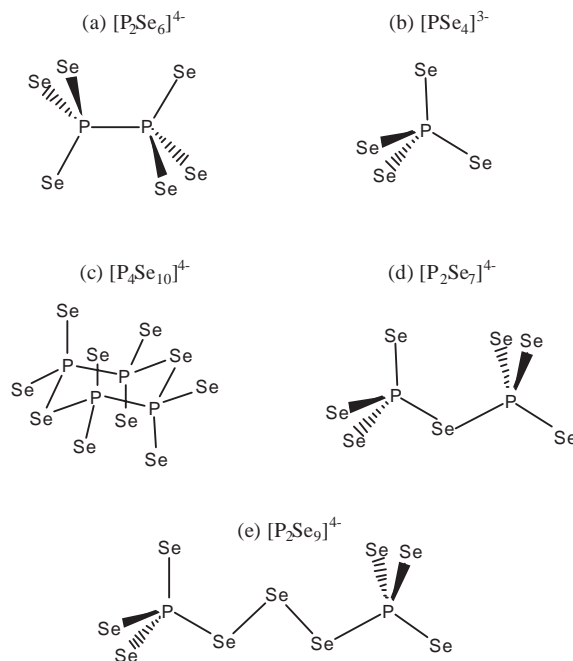(d) $[P_2Se_7]^{4-}$

(e) $[P_2Se_9]^{4-}$

Fig. 1. Schematic structures for various $[P_xSe_y]^{n-}$ anions examined. Reprinted with permission from C.G. Canlas, M.G. Kanatzidis, and D.P. Weliky, *Inorganic Chemistry*, American Chemical Society, 2003.

T_1 values which are close to one another. Unlike the CS, T_1 does not appear to correlate with P–P bonding.

3.2. Significance of relaxation times in compound identification

The importance of quantifying ^{31}P relaxation rates is demonstrated in Fig. 3, which presents the NMR analysis of the products of two Ag/P/Se reactions which were both run under the conditions described in Materials and Methods. The spectra in (a) and (b) are from one run of the reaction and the spectra in (c)–(f) are from the second run of the reaction. For both reactions, the experimental X-ray powder diffraction pattern of the products was approximately quantitatively consistent with the pattern simulated from the known single-crystal structure of $Ag_4P_2Se_6$ (data not shown) [20]. However, NMR data clearly showed a significant Ag_7PSe_6 impurity, as displayed in Fig. 3. In these spectra, Ag_7PSe_6 resonates at –51 ppm while the two inequivalent ^{31}P in $Ag_4P_2Se_6$ resonate at 77.6 and 91.8 ppm [15, 17, 18]. At the short relaxation delays in (a) and (b), the spectra have a larger Ag_7PSe_6 peak while at the 10000 s delay in (f), this peak represents only about 20% of the total integrated signal intensity. Two significant conclusions can be drawn from these data. First, for these syntheses, ^{31}P NMR is a complementary tool to powder X-ray diffraction for compound identification and impurity analysis. In this case, the powder diffraction

Table 1
^{31}P chemical shift, chemical shift anisotropy, and T_1 measurements for metal selenophosphates[a]

Selenophosphate	Anion type	CS (ppm)[b]	CSA principal values (ppm)[c]			CSA (ppm)[d]	T_1 (s)[e]
			δ_{11}	δ_{22}	δ_{33}		
$Pb_2P_2Se_6$	$P_2Se_6^{4-}$	29.1	97	49	−59	156	1700 (100)
$Rb_2CdP_2Se_6$	$P_2Se_6^{4-}$	62.0	160	95	−68	229	80 (5)
$K_2CdP_2Se_6$	$P_2Se_6^{4-}$	63.3	173	82	−65	238	23 (2)
$Ag_4P_2Se_6$	$P_2Se_6^{4-}$	77.6	152	73	7	145	3000 (200)
		91.8	166	106	3	164	
$K_2Cu_2P_4Se_{10}$	$P_4Se_{10}^{4-}$	55.7	129	47	–9	138	1050 (100)
Ag_7PSe_6	PSe_4^{3-}, Se^{2-}	−51.9	n.d.	n.d.	n.d.	n.d.	1500 (50)
Cu_3PSe_4	PSe_4^{3-}	−83.3	n.d.	n.d.	n.d.	n.d.	300 (10)
$RbPbPSe_4$	PSe_4^{3-}	−74.9	−49	−64	−112	63	970 (75)
$KPbPSe_4$	PSe_4^{3-}	−74.3	−42	−62	−119	76	1080 (100)
$K_4Pb(PSe_4)_2$	PSe_4^{3-}	−113.2	−82	−107	−151	69	1250 (100)
$Cs_4P_2Se_9$	$P_2Se_9^{4-}$	−39.9	59	−54	−124	183	800 (200)
$Rb_4Ti_2P_6Se_{25}$[f]	$P2Se_9^{4-}$	−34.6	101	−34	−172	273	540 (50)
	$P2Se_9^{4-}$	−47.6	51	−58	−135	186	630 (40)
	$P2Se_7^{4-}$	−67.7	12	−65	−150	162	690 (50)

n.d. = not determined because of negligible spinning sideband intensity.

[a] Reprinted with permission from C.G. Canlas, M.G. Kanatzidis, and D.P. Weliky, *Inorganic Chemistry*, American Chemical Society, 2003.

[b] Uncertainties are $\sim \pm 0.5$ ppm.

[c] Uncertainties are $\sim \pm 10$ ppm.

[d] CSA $= \delta_{11} - \delta_{33}$. Uncertainties are $\sim \pm 20$ ppm.

[e] Uncertainties are given in parentheses.

[f] CS assignments were based on G. Regelsky, Ph. D. Thesis, University of Muenster, 2000.

patterns of the two phases were very similar and NMR was a better technique to investigate compound purity. Second, the large variation in ^{31}P relaxation rates among different compounds can lead to quantitatively distorted spectra at short relaxation delays. In this case, the data at short relaxation delays initially led to confusion in assignment of peaks to $Ag_4P_2Se_6$.

3.3. Dependence of relaxation rates on dipolar couplings

There are a wide variety of interactions which could contribute to ^{31}P longitudinal relaxation including CSA and dipolar couplings [27]. However, CSA does not appear to be a major factor, as evidenced by the lack of positive correlation between CSA and relaxation rate ($1/T_1$). For example, $RbPbPSe_4$, $KPbPSe_4$, and $K_4Pb(PSe_4)_2$ all have CSAs which are approximately half those observed for $Pb_2P_2Se_6$ and $Ag_4P_2Se_6$, yet the relaxation rates of the former compounds are two to three times greater than those of the latter compounds.

A second possibility is that homonuclear and heteronuclear dipolar couplings play a dominant role in relaxation. If this were the case, then there should be an approximately positive linear correlation between the dipolar coupling squared
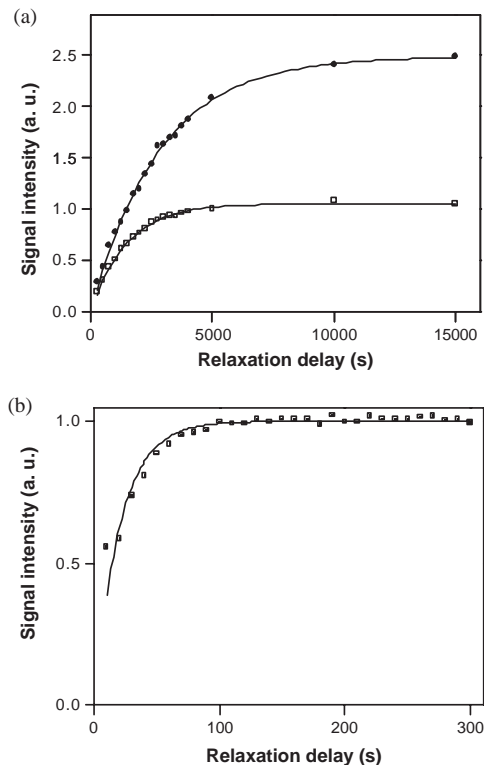
Fig. 2. (a) Experimental data and fitting of relaxation times for $Ag_4P_2Se_6$ (solid circles) and Ag_7PSe_6 (open squares). (b) Experimental data and fitting of relaxation time for $K_2CdP_2Se_6$. After nulling the magnetization, there was a variable relaxation delay (τ) followed by a 90° pulse and data acquisition. Signal intensities (in arbitrary units) were calculated as the sum of the integrated isotropic peak and spinning sidebands. Fitting was done using Eq. (1) and the best-fit curves are superimposed on the experimental data. Among all of the compounds in the present study, $Ag_4P_2Se_6$ and $K_2CdP_2Se_6$ had the slowest and fastest relaxation rates, respectively. Fig. 2(a) is reprinted with permission from C.G. Canlas, M.G. Kanatzidis, and D.P. Weliky, *Inorganic Chemistry*, American Chemical Society, 2003.

$(DC)^2$ and $1/T_1$ [27]. To test for this correlation, the former quantity was calculated using the following equation:

$$(DC)^2 = \Sigma \; 3/2(\gamma_P^4/r_{P-P}^6) + \Sigma \; 4B_J S_J^2(\gamma_P^2\gamma_J^2/r_{P-I}^6). \qquad (2)$$

This equation is based on an approximate model which considers that the total relaxation rate of a phosphorus nucleus (P) is the sum of relaxation rates from individual P–X dipolar interactions where X is a nearby nucleus. X could either be a phosphorus or another element type (I). In the right-hand side of Eq. (2), the first and second terms represent these homo- and heteronuclear squared dipolar couplings, respectively. In Eq. (2), r_{P-P} and r_{P-I} are internuclear distances determined from crystal structures [20–26], J represents one of the isotopes of element I, B_J is its fractional natural abundance, S_J is its spin quantum number, and γ_P and γ_J are the

gyromagnetic ratios of ^{31}P and J, respectively. The sums are over all isotopes of nearby homo- and heteronuclei. Eq. (2) only considers the squared dipolar coupling constants and neglects the angular dependences of the dipolar couplings, although presumably the significance of these anisotropic terms is reduced by powder
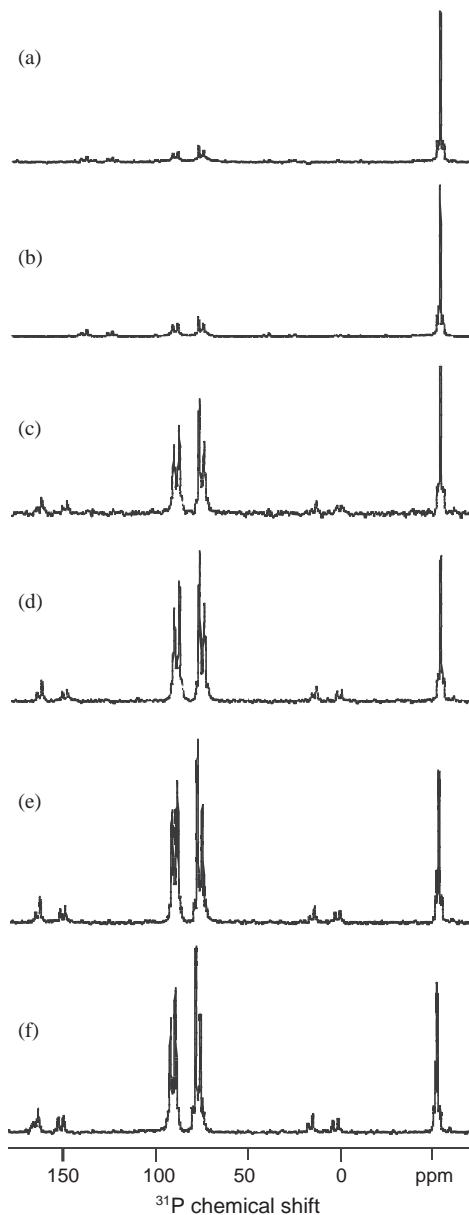
averaging. In addition, this model: (1) neglects the multiple magnitudes of azimuthal quantum numbers for quadrupolar spins and the resulting multiplicity of dipolar matrix elements; and (2) assumes that all compounds have similar ranges of motional correlation times.

Fig. 4 displays plots of $1/T_1$ vs. $(DC)^2$ for (a) compounds whose selenophosphate anion does not contain a P–P bond and (b) compounds whose selenophosphate anion contains a P–P bond. For the inset plot in (b), the four points nearest the abscissa are shown on an expanded vertical scale. In Fig. 4(a), there is an approximate positive linear correlation between the two variables. Interestingly, the intercept on the ordinate axis corresponds to a non-zero relaxation rate, which is physically reasonable and could be due to some interaction other than dipolar coupling. In some contrast, if one considers all of the data in Fig. 4(b), the data do not fit well to a linear correlation. However, a clearer picture emerges if we consider the $1/T_1$ vs. $(DC)^2$ data as three groups: (1) group A which corresponds to the data in Fig. 4(a); (2) group B1, the four points nearest the abscissa of Fig. 4(b) (shown on an expanded vertical scale in the inset); and (3) group B2, the other two points in Fig. 4(b). In the subsequent section, we will discuss a possible mechanism for the very fast relaxation of group B2. In this section, we present a unified model for groups A and B1. First, as shown in the inset of Fig. 4(b), the group B1 data also show an approximate positive linear correlation. Furthermore, if the large P–P dipolar couplings are not included in the $(DC)^2$ calculation, then these B1 data generally fall within group A positive linear correlation displayed in Fig. 4(a). This latter observation suggests that modulation of the large directly bonded P–P dipolar coupling does not contribute greatly to relaxation. Because Se is 92% spin zero isotopes, P–Se couplings make only a small contribution to $(DC)^2$ for most compounds. Thus, groups A and B1 data are consistent with a large component of dipolar relaxation which is predominantly due to fluctuations in P–M couplings (M≡metal ion). Although the static P–M couplings are smaller than the directly bonded P–P coupling, the metal ions may have larger motional amplitudes and/or more efficient motional correlation times than the selenophosphate anions, and thus dominate dipolar relaxation. Metal ion NMR as well as temperature- and field-dependent studies may provide more insight into the interactions and motions which are associated with NMR relaxation.

Fig. 3. ^{31}P NMR spectra of products of Ag/P/Se syntheses. All of the spectra were taken at ambient temperature. The spectra in (a) and (b) are from one synthesis with relaxation delays of 100 and 200 s, respectively. Each spectrum represents the co-addition of 32 scans taken at 8 kHz MAS frequency. The spectra in (c)–(f) are from a different synthesis with relaxation delays of (c) 1000 s, (d) 2000 s, (e) 5000 s, and (f) 10000 s. Each of the (c)–(f) spectra represents a single FID which was taken after the listed relaxation delay and at 12 kHz MAS frequency. There are isotropic resonances for $Ag_4P_2Se_6$ in the 70–95 ppm range and an isotropic peak for Ag_7PSe_6 at –51 ppm. Spinning sidebands are also apparent for $Ag_4P_2Se_6$. Spectra are displayed so that the Ag_7PSe_6 peak always has the same height. At the short relaxation delays in (a) and (b), the spectra have a larger Ag_7PSe_6 peak while at the 10000 s delay in (f), this peak represents only about 20% of the total integrated signal intensity. All spectra were processed with 100 Hz line broadening.
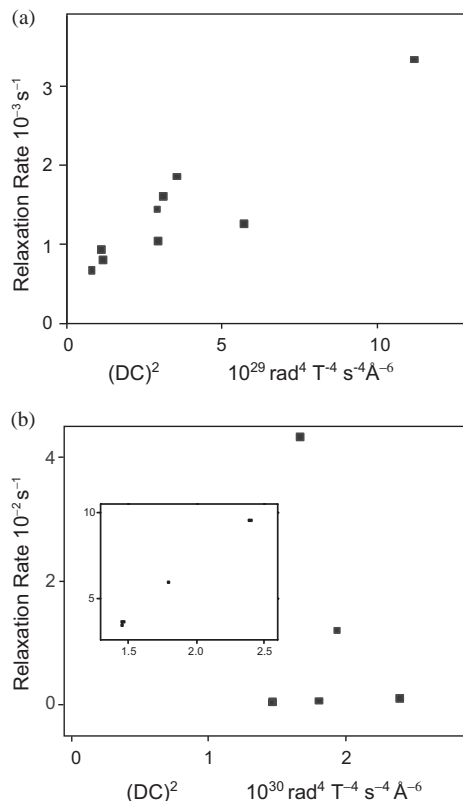
Fig. 4. Plots of ^{31}P $1/T_1$ vs. squared dipolar interaction. Data is displayed for (a) compounds whose selenophosphate anion does not contain a P–P bond and (b) compounds whose selenophosphate anion contains a P–P bond. The inset plot in (b) shows the four points closest to the abscissa on an expanded vertical scale whose unit is 10^{-4} s^{-1}. In each plot, the abscissa represents an approximate measure of the sum of the squares of the individual dipolar interactions between a central ^{31}P and the nearby nuclear spins. The dipolar sum calculation uses Eq. (2) and distances from known crystal structures.

3.4. Relaxation due to unpaired electrons

In Fig. 4(b), the rapid relaxation of group B2 (Rb$_2$CdP$_2$Se$_6$ and K$_2$CdP$_2$Se$_6$) suggests that there is an important relaxation mechanism for these compounds other than dipolar coupling. One reasonable possibility is relaxation caused by unpaired electrons. Although none of the compounds in this study is intrinsically paramagnetic, there is still the possibility that there are small but significant quantities of trapped paramagnetic impurities. To first test this hypothesis, we resynthesized the fast-relaxing Rb$_2$CdP$_2$Se$_6$ with the idea that paramagnetic reactant concentrations could vary between reactant batches, and thus produce different T_1 in the final products. The T_1 value for the resynthesized Rb$_2$CdP$_2$Se$_6$ was 70 s, which is close to but not the same as its 80 s value in the first synthesis.

A more definitive probe of the existence of unpaired electrons is electron spin resonance (ESR) [28] and Fig. 5 displays the ESR spectra of (a) $K_2CdP_2Se_6$ and (b) $Rb_2CdP_2Se_6$. Both samples showed significant ESR signals, including a sharp signal in the $g = 2$ region. These data imply that unpaired electrons could contribute to the ^{31}P relaxation rate. In future studies, we will quantitate the concentration of unpaired electrons and with a simple relaxation model, we should be able to determine whether this concentration is sufficient to explain the enhanced ^{31}P relaxation rate. It may also be possible to use electron-nuclear double resonance to determine the chemical identity of the paramagnetic impurities.

In summary, the ^{31}P T_1 varies by two orders of magnitude among different metal selenophosphate compounds. For compounds whose selenophosphate anion does not contain a P–P bond, there is an approximate positive linear correlation between squared dipolar couplings and relaxation rate. If we neglect P–P coupling, this correlation also holds for several compounds whose anion contains a P–P bond. These data suggest that P–metal ion dipolar fluctuations make a large contribution to ^{31}P relaxation in these materials. Two of the compounds, $Rb_2CdP_2Se_6$ and
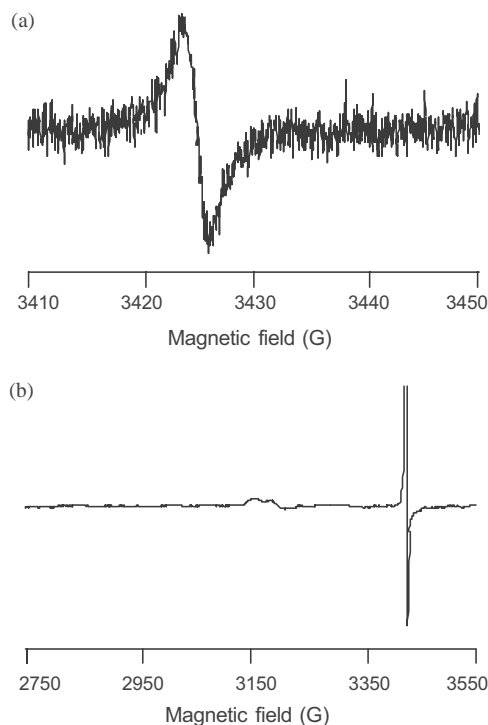

Fig. 5. X-band ESR spectra of (a) $K_2CdP_2Se_6$ and (b) $Rb_2CdP_2Se_6$ at 4.2 K. For $K_2CdP_2Se_6$, the spectrometer settings were: 100 kHz modulation frequency, 0.276 G modulation amplitude, 10.24 ms time constant, and 41.943 s sweep time. For $Rb_2CdP_2Se_6$, the spectrometer settings were: 100 kHz modulation frequency, 2.188 G modulation amplitude, 5.12 ms time constant, and 41.943 s sweep time. No ESR signals were observed for an empty cavity.

$K_2CdP_2Se_6$, appear to have a significant relaxation mechanism in addition to internuclear dipolar couplings. For these compounds, unpaired electrons were detected by ESR spectroscopy and may be the origin of enhanced ^{31}P relaxation. Finally, ^{31}P solid-state NMR is shown to be an important tool for impurity detection in these compounds. However, because of the large variation in relaxation rates among different compounds, spectra taken with short relaxation delays may be very non-quantitative, and this can cause difficulties in assignment of NMR peaks to particular synthetic products.

Acknowledgments

References

[1] M.G. Kanatzidis, New directions in synthetic solid state chemistry: chalcophosphate salt fluxes for discovery of new multinary solids, Curr. Opin. Solid State Mater. Sci. 2 (1997) 139–149.

[2] R. Clement, A novel route to intercalation into layered MnPS3, J. Chem. Soc. Chem. Commun. 14 (1980) 647–648.

[3] A. Michalowicz, R. Clement, Exafs study of the structural modifications induced into $MnPS_3$ upon intercalation, Inorg. Chem. 21 (1982) 3872–3877.

[4] M. Jansen, U. Henseler, Synthesis, structure determination, and ionic-conductivity of sodium tetrathiophosphate, J. Solid State Chem. 99 (1992) 110–119.

[5] P.G. Lacroix, R. Clement, K. Nakatani, J. Zyss, I. Ledoux, Stilbazolium-MPS_3 nanocomposites with large 2nd-order optical nonlinearity and permanent magnetization, Science 263 (1994) 658–660.

[6] G. Ouvrard, R. Brec, J. Rouxel, Structural determination of some $MnPS_3,FePS_3,CoPS_3,NiPS_3,CdPS_3$ layered phases, Mater. Res. Bull. 20 (1985) 1181–1189.

[7] B. Lerolland, P. McMillan, P. Molinie, P. Colombet, Synthesis and structural characterization of YPS_4, $GdPS_4$, $TbPS_4$, and $YbPS_4$, Eur. J. Solid State Inorg. Chem. 27 (1990) 715–724.

[8] M. Evain, R. Brec, M.H. Whangbo, Structural and electronic-properties of transition-metal thiophosphates, J. Solid State Chem. 71 (1987) 244–262.

[9] M. Evain, S. Lee, M. Queignec, R. Brec, Multiple empty tunnels in a new Ta–P–S phase—synthesis and structure determination of $Ta_2P_2S_{11}$, J. Solid State Chem. 71 (1987) 139–153.

[10] M. Evain, M. Queignec, R. Brec, J. Rouxel, $Ta_4P_4S_{29}$—A new tunnel structure with inserted polymeric sulfur, J. Solid State Chem. 56 (1985) 148–157.

[11] E.D. Rogach, E.A. Arnautova, E.A. Savchenko, N.A. Korchagina, L.P. Barinov, Stability of polarized condition of ferroelectric-films of $Sn_2P_2S_6$, Zh. Tekh. Fiz. 61 (1991) 164–167.

[12] X. Bourdon, A.R. Grimmer, V.B. Cajipe, P-31 MAS NMR study of the ferrielectric-paraelectric transition in layered $CuInP_2S_6$, Chem. Mater. 11 (1999) 2680–2686.

[13] A. Katty, S. Soled, A. Wold, Crystal-growth and characterization of $In_{2/3}PSe_3$, Mat. Res. Bull. 12 (1977) 663–666.

[14] M. Etman, A. Katty, C. Levyclement, P. Lemasson, Photo-electrochemical study of the layered compound $In_{2/3}PSe_3$, Mat. Res. Bull. 17 (1982) 579–584.

[15] R. Maxwell, D. Lathrop, D. Franke, H. Eckert, Heteronuclear X-Y decoupling in the Mas-NMR spectroscopy of inorganic solids, Ang. Chem. Int. Ed. 29 (1990) 882–884.

[16] R.H.P. Francisco, T. Tepe, H. Eckert, A study of the system Li–P–Se, J. Solid State Chem. 107 (1993) 452–459.

[17] R.H.P. Francisco, H. Eckert, Compound formation and local-structure in ternary metal-phosphorus-selenium systems, J. Solid State Chem. 112 (1994) 270–276.

[18] E. Gaudin, F. Boucher, M. Evain, F. Taulelle, NMR selection of space groups in structural analysis of Ag_7PSe_6, Chem. Mater. 12 (2000) 1715–1720.

[19] C.G. Canlas, M.G. Kanatzidis, D.P. Weliky, ^{31}P solid state NMR studies of metal selenophosphates containing $[P_2Se_6]^{4-}$, $[P_4Se_{10}]^{4-}$, $[PSe_4]^{3-}$, $[P_2Se_7]^{4-}$, and $[P_2Se_9]^{4-}$ ligands, Inorg. Chem. 42 (2003) 3399–3405.

[20] P. Toffoli, P. Khodadad, N. Rodier, Crystal-structure of silver hexaselenohypodiphosphate, $Ag_4P_2Se_6$, Acta Crystallogr. B: Struct. Sci. 34 (1978) 1779–1781.

[21] H. Yun, J.A. Ibers, Structure of $PbPSe_3$, Acta Crystallogr. C: Cryst. Struct. Commun. 43 (1987) 2002–2004.

[22] J. Garin, E. Parthe, The crystal structure of Cu_3PSe_4 and other ternary normal tetrahedral structure compounds with composition 13564, Acta Crystallogr. B 28 (1972) 3672.

[23] K. Chondroudis, T.J. McCarthy, M.G. Kanatzidis, Chemistry in molten alkali metal polyselenophosphate fluxes. Influence of flux composition on dimensionality. Layers and chains in $APbPSe_4$, $A_4Pb(PSe_4)_2$ (A = Rb, Cs) and $K_4Eu(PSe4)_2$, Inorg. Chem. 35 (1996) 840–844.

[24] K. Chondroudis, M.G. Kanatzidis, Flux synthesis of $K_2Cu_2P_4Se_{10}$: a layered selenophosphate with a new cyclohexane-like $[P_4Se_{10}]^{4-}$ group, Inorg. Chem. 37 (1998) 2098–2099.

[25] K. Chondroudis, M.G. Kanatzidis, Group 10 and group 12 one-dimensional selenodiphosphates: $A_2MP_2Se_6$ (A = K, Rb, Cs; M = Pd, Zn, Cd, Hg), J. Solid State Chem. 138 (1998) 321–328.

[26] K. Chondroudis, M.G. Kanatzidis, Complex multinary compounds from molten alkali-metal polyselenophosphate fluxes—layers and chains in $A_4Ti_2(P_2Se_9)_2(P_2Se_7)$ and $ATiPSe_5$ (A = K, Rb) - Isolation of $[P_2Se_9]^{4-}$ a flux constituent anion, Inorg. Chem. 34 (1995) 5401–5402.

[27] R.K. Harris, Nuclear Magnetic Resonance Spectroscopy, Wiley, New York, 1986.

[28] A. Carrington, A.D. McLachlan, Introduction to Magnetic Resonance with Applications to Chemistry and Chemical Physics, Harper, New York, 1967.